Original Russian Text © S. G. Demyshev, 2022,
published in MORSKOY GIDROFIZICHESKIY ZHURNAL, Vol. 38, Iss. 3 (2022)

Discrete Equation for the Available Potential Energy as an Exact Consequence of the Numerical Model Equations

S. G. Demyshev ✉

Marine Hydrophysical Institute of RAS, Sevastopol, Russian Federation
✉ *demyshev@gmail.com*

Abstract

Purpose. The work is aimed at obtaining a discrete equation for the rate of the available potential energy change in strict accordance with the finite-difference formulation that ensures adequate reproduction of discrete energy, and at analyzing its terms based on the results of a numerical experiment with realistic atmospheric forcing.

Methods and Results. On the basis of the well-known methods of computational mathematics (method of indeterminate coefficients and imitation modeling), a finite-difference equation for the available potential energy, which corresponded to its differential form, was obtained. In the equation structure, an additional term, which was conditioned by transition to a discrete problem and had a diffusion form, appeared. Energy analysis for the hydrological winter of 2011 in the Black Sea showed that the highest values of available potential energy in the upper layer were observed in the central region of the sea. Below 100 m, the available potential energy increased towards the coast where intense mesoscale variability was observed. At the depths exceeding 200 meters, the largest stock of this energy was concentrated in the Sevastopol and Batumi anticyclones. Action of the main forces, namely the forces of buoyancy, advection and horizontal diffusion, takes place in the coastal areas of the sea.

Conclusions. The resulting difference equation for the rate of the available potential energy change exactly corresponds to the discrete formulation and, therefore, accurately reflects the energy of the discrete problem. Analysis of the equation permitted to show that in winter, the rate of the available potential energy change is influenced predominantly by eddy activity at the depth slope.

Keywords: numerical simulation, available potential energy, potential energy, Black Sea, cyclonic circulation, anticyclonic eddies, discrete energy equation, difference equation

Acknowledgments: the investigation was carried out within the framework of the state assignment on theme No. 0555-2021-0004 “Fundamental studies of oceanological processes determining state and evolution of marine environment under the influence of natural and anthropogenic factors, based on the observation and modeling methods”.

For citation: Demyshev, S.G., 2022. Discrete Equation for the Available Potential Energy as an Exact Consequence of the Numerical Model Equations. *Physical Oceanography.* 29(3), pp. 221-236. doi:10.22449/1573-160X-2022-3-221-236

DOI: 10.22449/1573-160X-2022-3-221-236

Introduction

Currently, an increasing attention is paid to the analysis of the energy of numerical experiments on the circulation simulation in the seas and oceans, since it allows the direct estimation of the role of the main forces in the circulation variability processes. Evaluation of the eddy and average energy balance helps to understand the way movements of different scales interact and what forces are decisive in this process.

In [1], the kinetic energy budget components in the World Ocean models are calculated depending on the horizontal resolution and horizontal viscosity. When

calculating the energetics, direct and reverse energy cascades are more accurately described in a model that reproduces structures with dimensions smaller than the Rossby baroclinic deformation radius. Based on the seasonal variability estimate of the eddy kinetic energy, the authors of [2] analyze the mesoscale variability of the velocity field. Energy analysis of currents in semi-enclosed seas permits to study the Kuroshio current dynamics [3] and the eddy activity evolution in the Red Sea [4]. In [5], based on an eddy-resolving model, the causes and evolution of the mesoscale variability of the Sea of Okhotsk circulation are analyzed. To that end, the kinetic energy budget is calculated and analyzed. It is shown that the generation of mesoscale features of the alongshore circulation is mainly due to baroclinic instability.

In classical work of E. Lorenz [6], the concept of available potential energy is introduced as a part of potential energy that can be converted into kinetic energy and vice versa. The sum of the kinetic and available potential energy is a new invariant that is preserved in the absence of external sources, friction and diffusion. By introducing the time-averaged energy and eddy energy concepts as deviations from the average [7, 8], it is possible to construct an energy cycle allowing to estimate the processes of interaction between average and eddy motions in the seas and oceans. The traditional method for approximating the equations for the rate of the kinetic and available potential energy change is the discretization of differential energy equations. In this case, strictly speaking, the finite difference energy equations do not correspond to the discrete equations of the model, which can lead to inaccurate quantitative estimates. A more correct approach should be the derivation of energy equations from the difference equations of the problem.

In [9], finite-difference equations for the rate of kinetic and potential energy change were obtained from the original discrete formulation and, on their basis, energy-active regions of the Black Sea climatic circulation were studied. The present work is a continuation of these studies. It is devoted to the derivation and analysis of the equation for the available potential energy as an exact consequence of the discrete equations of the model. Using the winter period of 2011 as an example, the energy terms of the equations for the available potential energy are calculated and their structure is analyzed.

Model equations and boundary conditions

The equations of the Black Sea dynamics model in the Boussinesq approximation, sea water hydrostatics and incompressibility have the following form [9]

$$u_t - (\xi + f)v + wu_z = -g\varsigma_x - \frac{1}{\rho_0}(P' + E)_x + \left(\nu_V u_z\right)_z - \nu_H \nabla^4 u, \tag{1}$$

$$v_t + (\xi + f)u + wv_z = -g\varsigma_y - \frac{1}{\rho_0}(P' + E)_y + \left(\nu_V v_z\right)_z - \nu_H \nabla^4 v, \tag{2}$$

$$u_x + v_y + w_z = 0, \tag{3}$$

$$P = g\rho_0\varsigma + g\int_0^z \rho d\mu = g\rho_0\varsigma + P', \tag{4}$$

$$T_t + (uT)_x + (vT)_y + (wT)_z = -\kappa^H \nabla^4 T + (\kappa^V T_z)_z, \tag{5}$$

$$S_t + (uS)_x + (vS)_y + (wS)_z = -\kappa^H \nabla^4 S + (\kappa^V S_z)_z, \tag{6}$$

$$\rho = \varphi(T, S). \tag{7}$$

Designations in the relations (1)–(7) are generally accepted [9]. The form of φ function in expression (7) will be specified later.

When $z = 0$

$$\nu_v u_z = -\tau^x,\ \nu_v v_z = -\tau^y,\ w = -\varsigma_t,\ \kappa^v T_z = Q^T,\ \kappa^V S_z = (Pr - Ev)S_0, \tag{8}$$

while $z = H(x, y)$

$$u = v = w = 0, \quad T_z = S_z = 0. \tag{9}$$

On solid sidewalls for meridional sections of the boundary

$$u = \nabla^2 u = v_x = \nabla^2 v_x = 0, \quad T_x = S_x = 0, \tag{10.1}$$

for the zonal ones –

$$v = \nabla^2 v = v_y = \nabla^2 v_y = 0, \quad T_y = S_y = 0. \tag{10.2}$$

In the boundary sections where rivers and the lower Bosphorus current flow in, the following conditions are set:
for meridional sections –

$$u = \nabla^2 u = v_y = \nabla^2 v_x = 0, \quad T = T^p, \quad S = S^p. \tag{11.1}$$

for the zonal ones –

$$v = \nabla^2 v = u_y = \nabla^2 u_y = 0, \quad T = T^p, \quad S = S^p. \tag{11.2}$$

Conditions (10) are satisfied for the upper Bosphorus current.

In the relations (8)–(11), the following designations are used: (τ^x, τ^y) is the tangential wind stress; $Q^T(x, y, t)$ is the heat flow; S_0 is the salinity on the sea surface obtained in the model; $Pr(x, y, t)$ is the precipitation; $Ev(x, y, t)$ is evaporation on the sea surface; (T^p, S^p) are the temperature and salinity at the mouths of the rivers and in the lower Bosphorus current set according to the results of observations.

Equations (1)–(7) are supplemented in accordance with the Mellor – Yamada 2.5 parametrization [10] with equations for the turbulence kinetic energy and the turbulence macroscale with the corresponding boundary and initial conditions.

The initial conditions for problem (1)–(11) were taken in the following form [11]:

when $t = t_0$

$$(T, S) = (T^0, S^0), \quad u = u^0, \quad v = v^0, \quad \zeta = \zeta^0. \tag{12}$$

Derivation of the difference equation of the rate of available potential energy change

Let us consider the problem in the absence of external forces and diffusion (in the adiabatic approximation). We believe that

$$\rho(x, y, z, t) = \rho^*(x, y, z, t) + \rho^S(z),$$

where

$$\rho^S(z) = \frac{1}{T}\int_T \left(\frac{1}{\Omega}\iint_S \rho(x, y, z, t) d\Omega \right) dt, \; d\Omega = dxdy, \tag{13}$$

where Ω is the integration domain at z-level; T is the integration time (in our case it is equal to one year).

Let us introduce the following notation:

$$A^{pe} = a^{pe}\left(\rho_z^S\right)^{-1}, \text{ where } \quad a^{pe} = g\frac{\left(\rho^*\right)^2}{2}.$$

The density equation is

$$\rho_t + \left(u\rho\right)_x + \left(v\rho\right)_y + \left(w\rho\right)_z = 0. \tag{14}$$

Substituting expansion (13) into expression (14), we obtain

$$\rho_t^* + u\rho_x^* + v\rho_y^* + w\rho_z^* + w\rho_z^S + \rho^*(u_x + v_y + w_z) = 0. \tag{15}$$

Transforming expression (15), we obtain an equation for the available potential energy.

$$\begin{aligned} &A_t^{pe} + \left[\left(ua^{pe}\right)_x + \left(va^{pe}\right)_y + \left(wa^{pe}\right)_z\right]\left(\rho_z^S\right)^{-1} + \\ &+ g\rho^* w + a^{pe}(u_x + v_y + w_z)\left(\rho_z^S\right)^{-1} = 0. \end{aligned} \tag{16}$$

In differential form, due to the continuity equation fulfillment, the last terms in the equations (15) and (16) are equal to zero. In the difference formulation, this may not be the case due to the approximation inconsistency ρ_z^S as a factor for horizontal and vertical advection.

Let us introduce the following notation (similarly for j, k) for an arbitrary grid function defined at i, j and k points (Fig. 1)

$$z_{k+1/2} = \frac{z_{k+1} + z_k}{2}, \quad h_z^{k+1/2} = z_{k+1} - z_k, \quad h_z^k = z_{k+1/2} - z_{k-1/2},$$

$$\delta_x \varphi_{i,j,k} = \frac{\varphi_{i+1/2,j,k} - \varphi_{i-1/2,j,k}}{h_x}, \quad \nabla^2_{x,y}\varphi_{i,j,k} = \delta^2_x \varphi_{i,j,k} + \delta^2_y \varphi_{i,j,k},$$

$$\nabla^4_{x,y}\varphi_{i,j,k} = \nabla^2_{x,y}\left(\nabla^2_{x,y}\varphi_{i,j,k}\right).$$

Let us write out finite-difference analogues of equations (3), (5) and (6):

$$\delta_x u_{i,j,k} + \delta_y v_{i,j,k} + \delta_z w_{i,j,k} = 0, \tag{17}$$

$$\frac{\partial T_{i,j,k}}{\partial t} + \delta_x\left(u_{i,j,k}T_{i,j,k}\right) + \delta_y\left(v_{i,j,k}T_{i,j,k}\right) + \delta_z\left(w_{i,j,k}T_{i,j,k}\right) = 0, \tag{18}$$

$$\frac{\partial S_{i,j,k}}{\partial t} + \delta_x\left(u_{i,j,k}S_{i,j,k}\right) + \delta_y\left(v_{i,j,k}S_{i,j,k}\right) + \delta_z\left(w_{i,j,k}S_{i,j,k}\right) = 0. \tag{19}$$

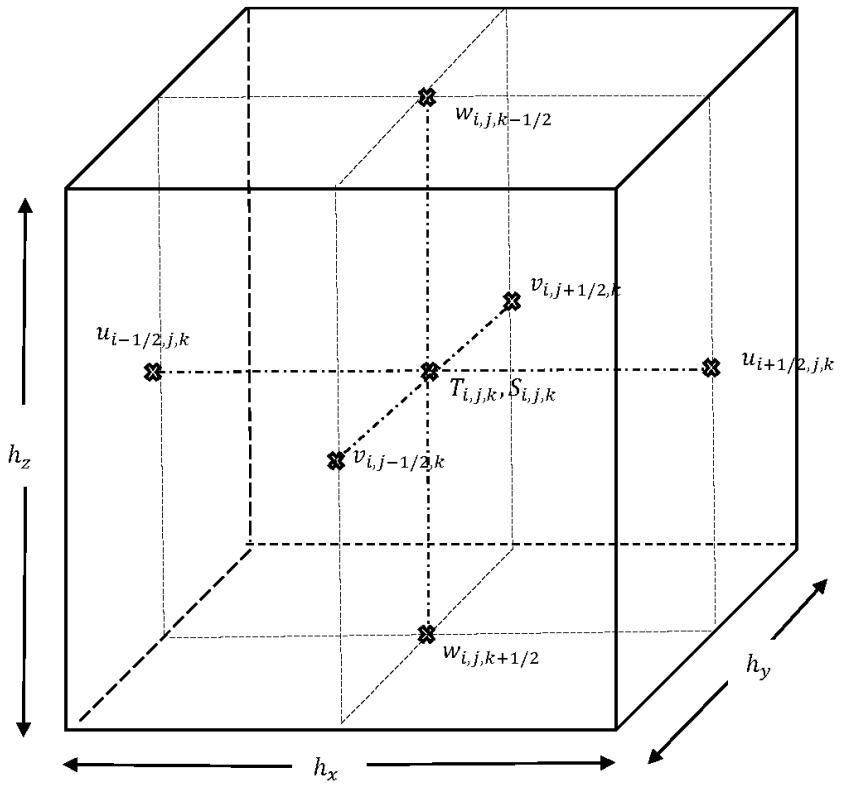

F i g. 1. Schematic image of the box (*i*, *j*, *k*) and spatial distribution of the variables

The equation for the density difference analogue in the adiabatic approximation has the following form

$$\frac{\partial \rho_{i,j,k}}{\partial t} + \delta_x\left(u_{i,j,k}\rho_{i,j,k}\right) + \delta_y\left(v_{i,j,k}\rho_{i,j,k}\right) + \delta_z\left(w_{i,j,k}\rho_{i,j,k}\right) = 0. \tag{20}$$

Let us introduce a discrete analog in the expansion (13):

$$\rho^{s}_{k+1/2} = \frac{1}{(t_2 - t_1)} \sum_{t_1}^{t_2} \frac{1}{\Omega_{\kappa+1/2}} \left(\sum_{i,j} \rho_{i,j,k+1/2} h_x h_y \right) h_t,$$

where h_t is the time step; $\Omega_{\kappa+1/2}$ – surface area at $z_{\kappa+1/2}$ level; t_1 is the initial and t_2 is the final moment of integration.

We believe that the expansion (13) can be written in discrete form as follows:

$$\rho_{i,j,k} = \rho^{*}_{i,j,k} + \rho^{s}_{k}, \quad \rho_{i+1/2,j,k} = \rho^{*}_{i+1/2,j,k} + \overline{\rho^{s}_{k}}^{z},$$

$$\rho_{i,j+1/2,k} = \rho^{*}_{i,j+1/2,k} + \overline{\rho^{s}_{k}}^{z} \qquad \rho_{i,j,k+1/2} = \rho^{*}_{i,j,k+1/2} + \rho^{s}_{k+1/2}. \qquad (21)$$

Substituting the expressions (21) into the formula (20) and taking into account difference equations (17)–(19), we obtain an analog of the equation (15):

$$\frac{\partial \rho^{*}_{i,j,k}}{\partial t} + \delta_x \left(u_{i,j,k} \rho^{*}_{i,j,k} \right) + \delta_y \left(v_{i,j,k} \rho^{*}_{i,j,k} \right) + \delta_z \left(w_{i,j,k} \rho^{*}_{i,j,k} \right) +$$

$$+ \overline{\rho^{s}_{k}}^{z} \left(\delta_x u_{i,j,k} + \delta_y v_{i,j,k} + \delta_z w_{i,j,k} \right) = -\overline{w_{i,j,k}}^{z} \delta_z \rho^{s}_{k}. \qquad (22)$$

Density approximations in the center and on the edges of the box depend on temperature and salinity, which in turn satisfy the nonlinear equation of state. To match the difference analogs $\rho_{i,j,k}, \rho_{i,j,k+1/2}$ with $T_{i,j,k}, T_{i,j,k+1/2}, S_{i,j,k}, S_{i,j,k+1/2}$, special relations were obtained [9]. It follows from them that $\overline{\rho^{s}_{k}}^{z} \neq \rho^{s}_{k}$. Therefore, the form of expression (22), in which the last term on the left side is equal to zero, is provided by an approximation of equation (21).

We believe that the equation of state is written as follows:

$$\rho_{i,j,k} = \sum_{n=0}^{2} \sum_{m=0}^{1} a_{nm} T^{n}_{i,j,k} S^{m}_{i,j,k} = a_{00} + a_{10} T_{i,j,k} + a_{01} S_{i,j,k} +$$

$$+ a_{11} T_{i,j,k} S_{i,j,k} + a_{20} T^{2}_{i,j,k}. \qquad (23)$$

Then, considering the density as a functional of $T_{i,j,k}$ and $S_{i,j,k}$ and differentiating the equation (23), we obtain

$$\left(\rho_{i,j,k} \right)'_{T} = a_{10} + a_{11} S_{i,j,k} + 2 a_{20} T_{i,j,k}, \quad \left(\rho_{i,j,k} \right)'_{S} = a_{01} + a_{11} T_{i,j,k}.$$

The expressions for calculating the density on the box faces [9] have the following form:

$$\rho_{i+1/2,j,k} = \alpha_{10}\overline{T_{i+1/2,j,k}}^{x} + \alpha_{01}\overline{S_{i+1/2,j,k}}^{x} + \alpha_{20}T_{i+1,j,k}T_{i,j,k} + \\ +\alpha_{11}\frac{T_{i,j,k}S_{i+1,j,k} + T_{i+1,j,k}S_{i,j,k}}{2},$$

$$\rho_{i,j+1/2,k} = \alpha_{10}\overline{T_{i,j+1/2,k}}^{y} + \alpha_{01}\overline{S_{i,j+1/2,k}}^{y} + \alpha_{20}T_{i,j+1,k}T_{i,j,k} + \\ +\alpha_{11}\frac{T_{i,j,k}S_{i,j+1,k} + T_{i,j+1,k}S_{i,j,k}}{2}, \qquad (24)$$

$$\rho_{i,j,k+1/2} = \alpha_{10}\overline{T_{i,j,k+1/2}}^{z} + \alpha_{01}\overline{S_{i,j,k+1/2}}^{z} + \alpha_{20}T_{i,j,k+1}T_{i,j,k} + \\ +\alpha_{11}\frac{T_{i,j,k}S_{i,j,k+1} + T_{i,j,k+1}S_{i,j,k}}{2}.$$

Then, taking into account the representation (24), we obtain

$$\overset{*}{\rho}_{i,j,k} = \overline{\overset{*}{\rho}_{i,j,k}}^{x} - \varphi^{x}_{i,j,k},\ \rho_{i,j,k} = \overline{\overset{*}{\rho}_{i,j,k}}^{y} - \varphi^{y}_{i,j,k},\ \overset{*}{\rho}_{i,j,k} = \overline{\overset{*}{\rho}_{i,j,k}}^{z} - \varphi^{z}_{i,j,k}, \qquad (25)$$

где

$$\varphi^{x}_{i,j,k} = \frac{h_x^2}{4}\left[\left(\overset{*}{\rho}_{i,j,k}\right)'_{T}\delta_x^2 T_{i,j,k} + \left(\overset{*}{\rho}_{i,j,k}\right)'_{S}\delta_x^2 S_{i,j,k}\right],$$

$$\varphi^{y}_{i,j,k} = \frac{h_y^2}{4}\left[\left(\overset{*}{\rho}_{i,j,k}\right)'_{T}\delta_y^2 T_{i,j,k} + \left(\overset{*}{\rho}_{i,j,k}\right)'_{S}\delta_y^2 S_{i,j,k}\right],$$

$$\varphi^{z}_{i,j,k} = \frac{h_z^k}{4}\left[\left(\overset{*}{\rho}_{i,j,k}\right)'_{T}\delta_z\left(h_z^k\delta_z T_{i,j,k}\right) + \left(\overset{*}{\rho}_{i,j,k}\right)'_{S}\delta_z\left(h_z^k\delta_z S_{i,j,k}\right)\right].$$

We believe that

$$A^{pe}_{i,j,k} = a^{pe}_{i,j,k}\left(\delta_z\rho^s_k\right)^{-1},\ \text{где}\quad a^{pe}_{i,j,k} = g\frac{\left(\overset{*}{\rho}_{i,j,k}\right)^2}{2}, \qquad (26)$$

$$a^{pe}_{i+1/2,j,k} = g\frac{\left(\overset{*}{\rho}_{i+1/2,j,k}\right)^2}{2},\ a^{pe}_{i,j+1/2,k} = g\frac{\left(\overset{*}{\rho}_{i,j+1/2,k}\right)^2}{2},$$

$$a^{pe}_{i,j,k+1.2} = g\frac{\left(\overset{*}{\rho}_{i,j,k+1.2}\right)^2}{2}.$$

Having carried out simple transformations, we obtain the following equation (analogous to the equation (16)):

$$\frac{\partial A^{pe}{}_{i,j,k}}{\partial t} + \left\{\delta_x\left(u_{i,j,k}a^{pe}_{i,j,k}\right) + \delta_y\left(v_{i,j,k}a^{pe}_{i,j,k}\right) + \delta_z\left(w_{i,j,k}a^{pe}_{i,j,k}\right)\right\}\left(\delta_z\rho_k\right)^{-1} +$$

$$+\frac{g}{2}\Big[\rho^{*}_{i+1/2,j,k}\rho^{*}_{i-1/2,j,k}\delta_x u_{i,j,k}+\rho^{*}_{i,j+1/2,k}\rho^{*}_{i,j-1/2,k}\delta_y v_{i,j,k}+$$
$$+\rho^{*}_{i,j,k+1/2}\rho^{*}_{i,j,k-1/2}\delta_z w_{i,j,k}\Big](\delta_z\rho_k)^{-1}= \quad (27)$$
$$=-g\,\overline{w_{i,j,k}}^{z}\rho^{*}_{i,j,k}+g\Big[\varphi^{x}_{i,j,k}\delta_x\left(u_{i,j,k}\rho^{*}_{i,j,k}\right)+\varphi^{y}_{i,j,k}\delta_y\left(v_{i,j,k}\rho^{*}_{i,j,k}\right)+$$
$$+\varphi^{z}_{i,j,k}\delta_z\left(w_{i,j,k}\rho^{*}_{i,j,k}\right)\Big](\delta_z\rho_k)^{-1}.$$

Consider the terms in this equation. The first two on the left side of the equation (27) are clear. The third term in square brackets has no analogue in the differential equation and is an additional difference term after the expression (22) is multiplied by the expansion (25). Its origin is associated with the available potential energy representation on the box edges, which, strictly speaking, can be different, adopted in formulas (26). Therefore, it seems possible to find suitable expressions for $a^{pe}_{i+1/2,j,k}, a^{pe}_{i,j+1/2,k}, a^{pe}_{i,j,k+1/2}$ for more accurate equation (16) approximation.

The first term on the right side of the equation (27) describes the work of the buoyancy force, the second is an additional term, which, taking into account the expansion (25), has a diffusion form. Estimates show that its value is an order of magnitude smaller than physical diffusion. Therefore, if it is included in the diffusion term, then the solution result will change insignificantly.

Let us rewrite equations (20) and (27) taking into account the diffusion:

$$\frac{\partial\rho_{i,j,k}}{t}+\delta_x(u_{i,j,k}\rho_{i,j,k})+\delta_y(v_{i,j,k}\rho_{i,j,k})+\delta_z(w_{i,j,k}\rho_{i,j,k})= \quad (28)$$
$$=\left(D^{\rho}_{V}+D^{\rho}_{H}\right)_{i,j,k},$$

$$\frac{\partial A^{pe}_{i,j,k}}{\partial t}+\left\{\delta_x\left(u_{i,j,k}a^{pe}_{i,j,k}\right)+\delta_y\left(v_{i,j,k}a^{pe}_{i,j,k}\right)+\delta_z\left(w_{i,j,k}a^{pe}_{i,j,k}\right)\right\}(\delta_z\rho_k)^{-1}+ \quad (29)$$
$$+g\,\overline{w_{i,j,k}}^{z}\rho^{*}_{i,j,k}+\omega_{i,j,k}=\left(D^{ape}_{V}+D^{ape}_{H}\right)_{i,j,k},$$

where the corresponding terms are included in the horizontal and vertical difference diffusion, and $\omega_{i,j,k}$ have an obvious form.

Let us rewrite the equation (29) in symbolic form:

$$\frac{\partial A^{pe}_{i,j,k}}{\partial t}+\alpha_{i,j,k}+b_{i,j,k}+\omega_{i,j,k}=\left(D^{ape}_{V}+D^{ape}_{H}\right)_{i,j,k}. \quad (30)$$

In equations (28)–(30), the following notations are introduced:

$$\alpha_{i,j,k}=\left\{\delta_x\left(u_{i,j,k}a^{pe}_{i,j,k}\right)+\delta_y\left(v_{i,j,k}a^{pe}_{i,j,k}\right)+\delta_z\left(w_{i,j,k}a^{pe}_{i,j,k}\right)\right\}(\delta_z\rho_k)^{-1},$$

$$b_{i,j,k} = -g\,\overline{w_{i,j,k}}^{z}\,\rho^{*}_{i,j,k}.$$

$$\left(D_V^{\rho}\right)_{i,j,k} = \alpha_{10}\delta_z[\kappa^V_{i,j,k}(\delta_z T_{i,j,k})] + \alpha_{01}\delta_z[\kappa^V_{i,j,k}(\delta_z S_{i,j,k})] +$$

$$+2\alpha_{20}[\delta_z[\kappa^V_{i,j,k}\,\overline{T_{i,j,k}}^{z}(\delta_z T_{i,j,k})] +$$

$$+\alpha_{11}\left[\left[T_{i,j,k}\delta_z[\kappa^V_{i,j,k}(\delta_z S_{i,j,k})] + S_{i,j,k}\delta_z[\kappa^V_{i,j,k}(\delta_z T_{i,j,k})]\right],\right.$$

$$\left(D_H^{\rho}\right)_{i,j,k} = \kappa^H(\alpha_{10}\nabla^2_{xy}T_{i,j,k} + \alpha_{01}\nabla^2_{xy}S_{i,j,k} + 2\alpha_{20}T_{i,j,k}\nabla^2_{xy}T_{i,j,k} +$$

$$+\alpha_{11}[T_{i,j,k}\nabla^2_{xy}S_{i,j,k} + S_{i,j,k}\nabla^2_{xy}T_{i,j,k}]),$$

$$\left(D_V^{ape}\right)_{i,j,k} = g\rho^*_{i,j,k}\left(D_V^{\rho}\right)_{i,j,k}\left(\delta_z\rho^s_k\right)^{-1} +$$

$$+ g\frac{h^k_z}{4}\left[\left(\rho^*_{i,j,k}\right)'_T\delta_z\left(h^k_z\delta_z T_{i,j,k}\right) + \left(\rho^*_{i,j,k}\right)'_S\delta_z\left(h^k_z\delta_z S_{i,j,k}\right)\right]\delta_z\left(w_{i,j,k}\rho^*_{i,j,k}\right)\left(\delta_z\rho_k\right)^{-1},$$

$$\left(D_H^{ape}\right)_{i,j,k} = g\rho^*_{i,j,k}\left(D_H^{\rho}\right)_{i,j,k}\left(\delta_z\rho^s_k\right)^{-1} +$$

$$+g\left\{\frac{h^2_x}{4}\left[\left(\rho^*_{i,j,k}\right)'_T\delta^2_x T_{i,j,k} + \left(\rho^*_{i,j,k}\right)'_S\delta^2_x S_{i,j,k}\right] +\right.$$

$$\left.+\frac{h^2_y}{4}\left[\left(\rho^*_{i,j,k}\right)'_T\delta^2_y T_{i,j,k} + \left(\rho^*_{i,j,k}\right)'_S\delta^2_y S_{i,j,k}\right]\right\}\left(\delta_z\rho^s_k\right)^{-1}.$$

Results of numerical calculations

To analyze the terms of the equation for the rate of available potential energy change (29), which make the main contribution to the energy cycle, the results of calculations of the Black Sea circulation for realistic atmospheric conditions in 2011 [11] will be used. Horizontal resolution was 1.6 × 1.6 km. Vertical calculation was carried out on 27 horizons. The fields for the initial conditions (12) corresponded to January 1, 2011.

Note that ρ^s_k was calculated as the average vertical profile for the year.

For example, consider the winter circulation regime. In 2011, it was characterized by the distinct Black Sea Rim Current throughout the year, which intensified in winter-spring period and weakened in summer-autumn period (Fig. 2). Anticyclonic eddies of various horizontal scales and intensities were observed along its periphery. Dynamics of the Black Sea currents in 2011 was considered in detail in [11], so now we are to go on to the analysis of the available potential energy variability at this time of the year.

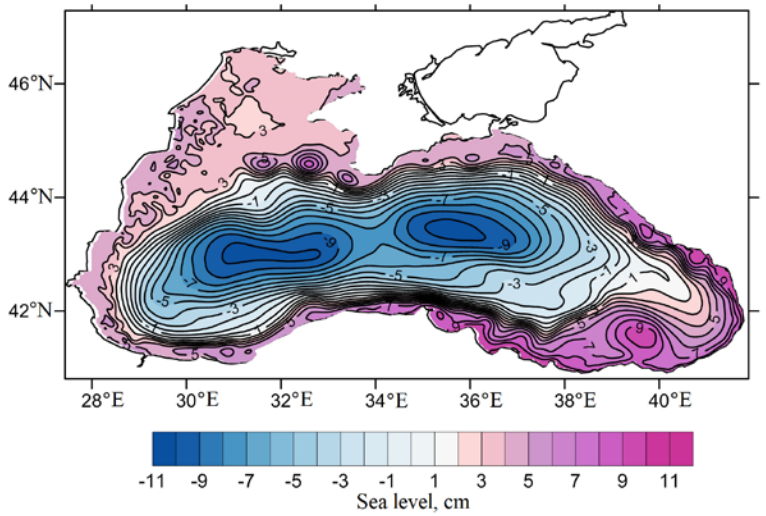

F i g. 2. Reducible sea level (cm) on February 1, 2011

Fig. 3 shows the horizontal structure of available potential energy for the middle of the hydrological winter of 2011. The horizon-averaged available potential energy decreases with depth and below the 50 m horizon, its value is an order of magnitude smaller than in the upper 30 m layer.

In the upper 30-meter layer in the central region of the sea (Fig. 3, *a*), corresponding to the cyclonic gyre center, higher values of available potential energy are observed, which decrease towards the periphery of the region. Below, the reverse trend takes place: in the sea center, the values are lower than on its periphery (Fig. 3, *b*, *c*). Moreover, in the deep layers (below the 200 m horizon), the largest supply of available potential energy takes place in anticyclonic gyres (the Sevastopol and Batumi ones). The local maximum available potential energy at the 50 m horizon (Fig. 3, *b*) is due to the inflow of the Marmara Sea waters.

Let us consider the structure of the main energy terms in the equation (29). The basic characteristic of energy exchange is the work of the buoyancy force, shown in Fig. 4.

Two distinct areas of kinetic and available potential energy exchange are observed: the central region of the sea, where this process occurs rather weakly, and the coastal area, characterized by intensive work of the buoyancy force. Moreover, the energy exchange patterns differ qualitatively in depth. In the upper 10–30 m layer (Fig. 4, *a*), the main work of the buoyancy force is concentrated along the western slope, where zones of transition from available potential energy to kinetic energy and vice versa exist. It indicates the possible development of various types of instability on the western continental slope. At the underlying horizons of the intensive work area, buoyancy forces are observed not only near the western coast, but also in the eastern regions – near the Anatolian and Caucasian coasts (Fig. 4, *b*, *c*). At depths of 200–300 m, in the zone of the Sevastopol and Batumi anticyclones, there is a clearly pronounced energy transition from kinetic to available potential energy, which indicates the baroclinic instability processes for this time period (Fig. 4, *c*).

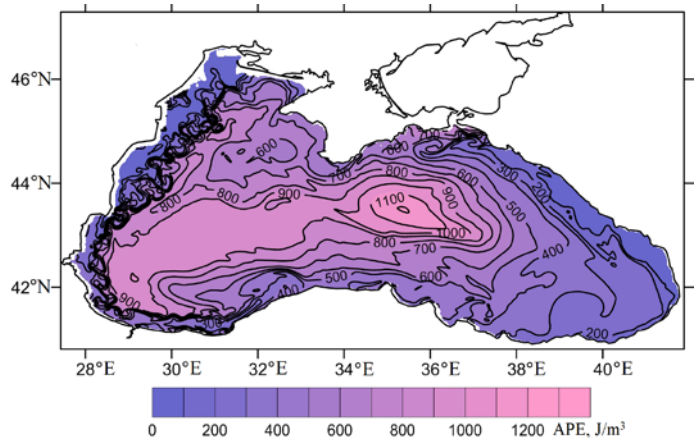

a

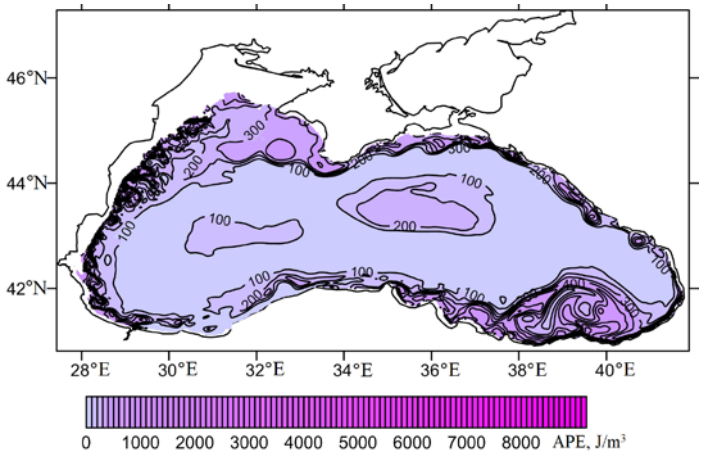

b

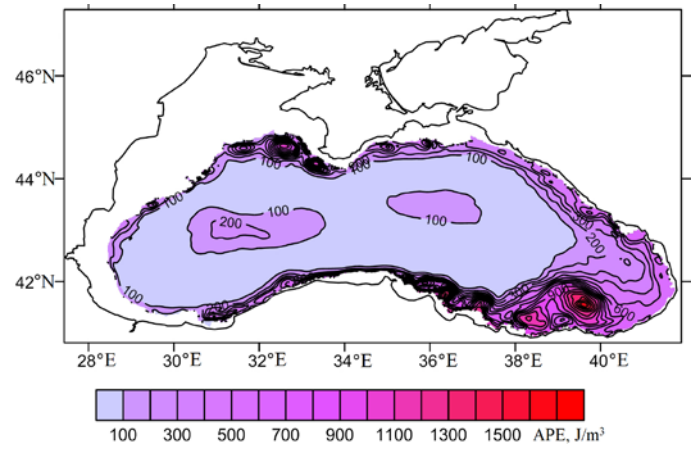

c

F i g. 3. Available potential energy at the 20 (*a*), 50 (*b*) and 300 m (*c*) horizons

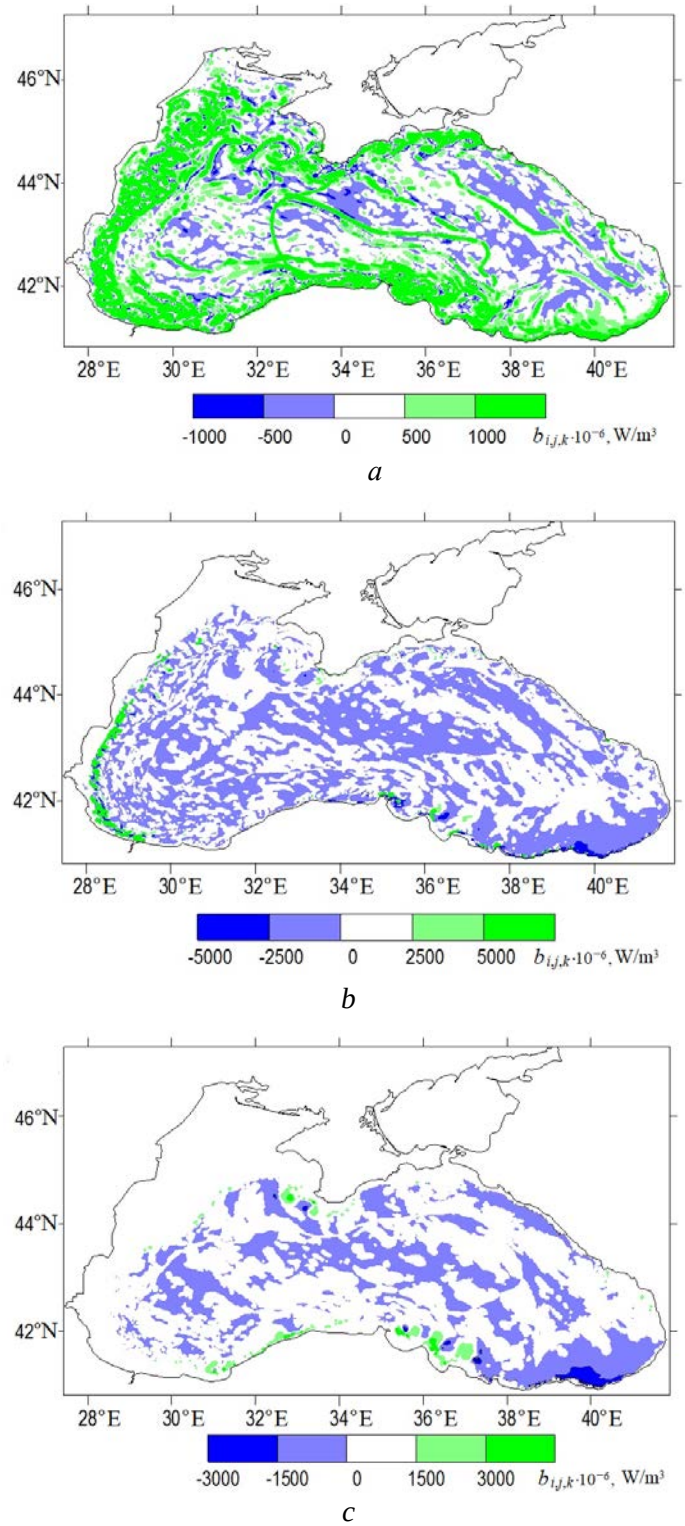

F i g. 4. Action of the buoyancy force at the 20 (*a*), 50 (*b*) and 300 m (*c*) horizons

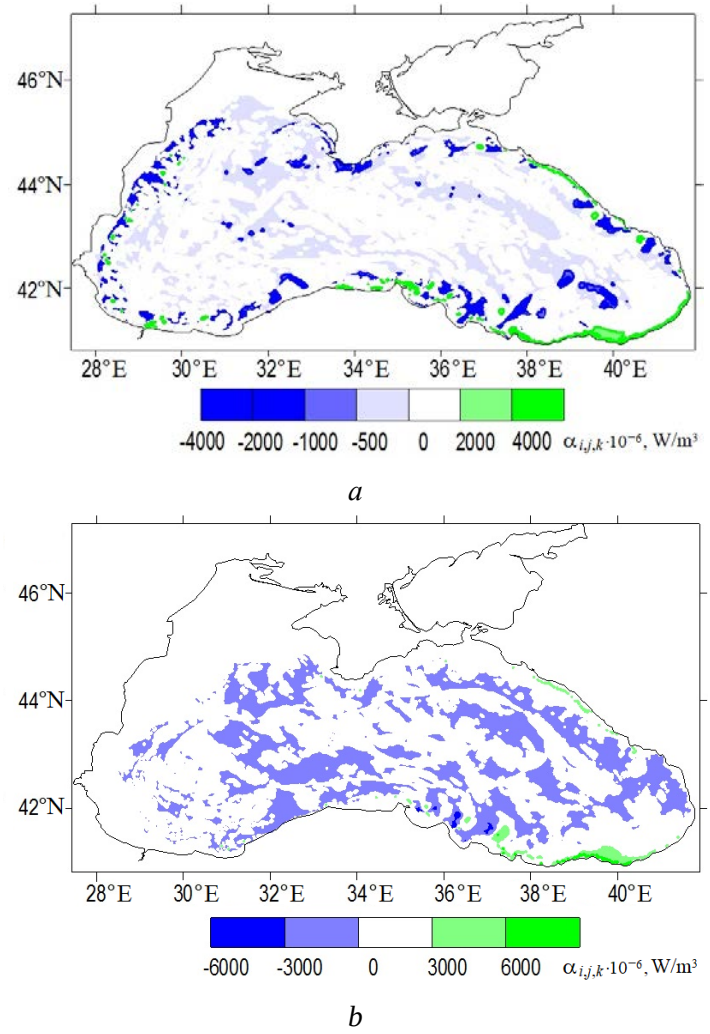

F i g. 5. Available potential energy advection at the 50 (*a*) and 300 m (*b*) horizons

The transfer of available potential energy as a result of advection (Fig. 5) occurs most intensively in the coastal sea area. In the upper 50-m layer, it is concentrated near the western coast, in the lower layers – along the Anatolian coast (Fig. 5, *a*). In contrast to the work of the buoyancy force in the area of the Sevastopol and Batumi anticyclones, the advection influence is small and rather uniform along the horizontal, which indicates an insignificant role of advective forces in the evolution of these gyres, at least during this time period. Below the 200 m horizon (Fig. 5, *b*), the greatest advective transport takes place in the Anatolian coast area (the zone of mesoscale eddies) and in the Sevastopol anticyclone area.

The greatest horizontal diffusion is observed in the upper layer of the sea (Fig. 6, *a*), which is influenced by two factors – significant horizontal gradients in the density field and the inflow of rivers, primarily the Danube. It is clear that, compared with the central part of the basin, the alongshore zone is characterized by

a large diffusion flux. This process is especially pronounced in deep layers (Fig. 6, *b*), where the available potential energy diffusion is concentrated near the side boundaries in the form of a narrow band.

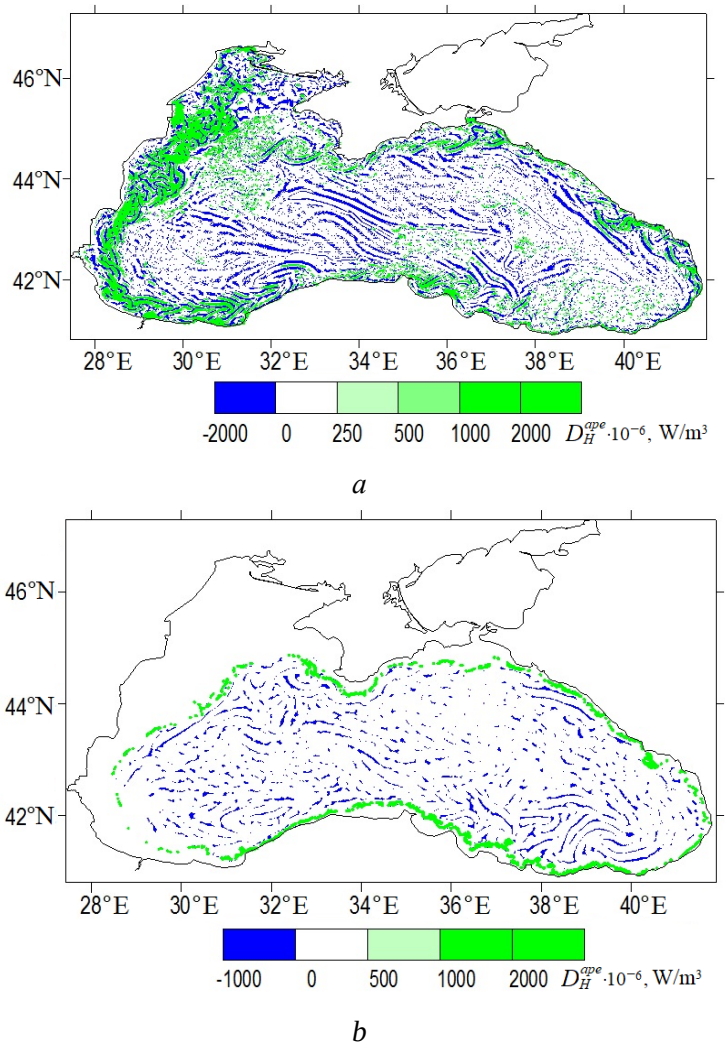

F i g. 6. Horizontal diffusion of available potential energy at the 5 (*a*) and 300 m (*b*) horizons

Structure of the vertical diffusion of available potential energy is determined primarily by the heat flows, precipitation and evaporation on the sea surface. Therefore, its greatest values are observed in the upper 20 m layer. Below D_V^{ape}, the values decrease by an order of magnitude.

Conclusion

To derive a discrete equation for the rate of available potential energy change, an overdetermined grid was used, where new unknown quantities connected by additional relations (21), (25), (26) were introduced. These connections were

chosen so that some properties of the differential problem were satisfied. Formulas (21) ensure the correspondence of the equations (15) and (22), expressions (25) and (26) lead to a finite difference equation (27), which includes a term that is not present in the differential formulation and has a diffusion form. Since it is an order of magnitude smaller than physical diffusion, it can be interpreted as additional diffusion, which, at least over a relatively short integration interval, does not affect the calculation results.

Based on the above, it can be argued that the problem of obtaining a discrete equation for available potential energy having the same characteristics as the continuous case has been partially completed. It is not necessary that the available potential energy on the box edges takes the form of the approximation (26). It can be assumed that there is a suitable choice of the expression (26), which will ensure the fulfillment of the basic properties of the differential equation.

The resulting difference equation (29) corresponds exactly to the discrete formulation and therefore adequately reflects the difference problem energetics. In the middle of the hydrological winter in the Black Sea, the highest values of available potential energy are observed in the upper layer in the sea center. Below the 100 m horizon, the picture is reversed – available potential energy increases towards the coast, where intense mesoscale variability is observed. At a depth over 200 m, the largest supply of available potential energy is concentrated in the Sevastopol and Batumi anticyclones. Therefore, for the winter period, it is typical that the available potential energy in the upper layer of the sea takes place in the central part of cyclonic gyres; at a depth of about 100 m or more, it is contained in the area of synoptic and mesoscale eddies.

Work of the main forces (buoyancy, advection and horizontal diffusion) is concentrated in the coastal sea areas. Thus, the rate of available potential energy change in the winter period is predominantly influenced by eddy activity at the continental slope.

REFERENCES

1. Kjellsson, J. and Zanna, L., 2017. The Impact of Horizontal Resolution on Energy Transfers in Global Ocean Models. *Fluids*, 2(3), 45. doi:10.3390/fluids2030045
2. Rieck, J.K., Bonning, C., Greatbatch, R.J. and Scheinert, M., 2015. Seasonal Variability of Eddy Kinetic Energy in a Global High-Resolution Ocean Model. *Geophysical Research Letters*, 42(21), pp. 9379-9386. doi:10.1002/2015GL066152
3. Yang, Y. and San Liang, X., 2018. On the Seasonal Eddy Variability in the Kuroshio Extension. *Journal of Physical Oceanography*, 48(8), pp. 1675-1689. doi:10.1175/JPO-D-18-0058.1
4. Zhan, P., Subramanian, A.C., Yao, F., Kartadikaria, A.R., Guo, D. and Hoteit, I., 2016. The Eddy Kinetic Energy Budget in the Red Sea. *Journal of Geophysical Research: Oceans*, 121(7), pp. 4732-4747. doi:10.1002/2015JC011589
5. Stepanov, D.V., Diansky, N.A. and Fomin, V.V., 2018. Eddy Energy Sources and Mesoscale Eddies in the Sea of Okhotsk. *Ocean Dynamics*, 68(7), pp. 825-845. doi:10.1007/s10236-018-1167-3
6. Lorenz, E.N., 1955. Available Potential Energy and the Maintenance of the General Circulation. *Tellus*, 7(2), pp. 157-167. doi:10.3402/TELLUSA.V7i2.8796
7. Holland, W.R., 1975. Energetics of Baroclinic Oceans. In: NAS, 1975. *Numerical Models of Ocean Circulation. Proceedings of a Symposium Held at Durham, New Hampshire, October 17-20, 1972*. Washington: National Academy Press, pp. 168-177.

8. Robinson, A.R., Harrison, D.E., Mintz, Y. and Semtner, A.J., 1977. Eddies and the General Circulation of an Idealized Oceanic Gyre: A Wind and Thermally Driven Primitive Equation Numerical Experiment. *Journal of Physical Oceanography*, 7(2), pp. 182-207. doi:10.1175/1520-0485(1977)007<0182:EATGCO>2.0.CO;2

9. Demyshev, S.G., 2004. Energy of the Black Sea Climatic Circulation. Part I: Discrete Equations of the Rate of Change of Kinetic and Potential Energy. *Meteorologiya i Gidrologiya*, 9, pp. 65-80 (in Russian).

10. Mellor, G.L. and Yamada, T., 1982. Development of a Turbulence Closure Model for Geophysical Fluid Problems. *Reviews of Geophysics*, 20(4), pp. 851-875. doi:10.1029/RG020I004P00851

11. Demyshev, S.G. and Dymova, O.A., 2018. Numerical Analysis of the Black Sea Currents and Mesoscale Eddies in 2006 and 2011. *Ocean Dynamics*, 68(10), pp. 1335-1352. doi:10.1007/s10236-018-1200-6

About the author:

Sergey G. Demyshev, Senior Research Associate, Head of Wave Theory Department, Marine Hydrophysical Institute of RAS (2 Kapitanskaya str., Sevastopol, 299011, Russian Federation), Dr.Sci. (Phys.-Math.), **ORCID ID: 0000-0002-5405-2282**, demyshev@gmail.ru

The author has read and approved the final manuscript.

The author declares that he has no conflict of interest.